

Article

Metal Rich Metallaboranes: Synthesis, Structure and Bonding of *pileo*-[(Cp**Ru*)₂M(CO)₃(μ -H)(μ -E)(μ ₃-BH)B₂H₅] (M = Mo, W, E = CO, and M = Mn, E = H) Clusters

Alaka Nanda Pradhan ¹, Shippy Jaiswal ¹, Marie Cordier ², Jean-François Halet ^{2,3,*} and Sundargopal Ghosh ^{1,*}

¹ Department of Chemistry, Indian Institute of Technology Madras, Chennai 600036, India; salupradhan7@gmail.com (A.N.P.); jaiswalshippy167@gmail.com (S.J.)

² Univ Rennes, CNRS, Ecole Nationale Supérieure de Chimie de Rennes, Institut des Sciences Chimiques de Rennes (ISCR), UMR 6226, F-35000 Rennes, France; marie.dallon@univ-rennes.fr

³ Laboratory for Innovative Key Materials and Structures (LINK), CNRS—Saint-Gobain—NIMS, IRL 3629, National Institute for Materials Science (NIMS), Tsukuba 305-0044, Japan

* Correspondence: jean-francois.halet@univ-rennes.fr (J.-F.H.); sghosh@iitm.ac.in (S.G.); Tel.: +91-44-225-742-30 (S.G.)

Abstract: The synthesis and structural characterization of a series of heterotrimetallic ruthenaborane clusters are reported. The photolytic reaction of *nido*-[(Cp**Ru*)₂(μ -H)₂B₃H₇] (*nido*-1) (Cp* = 1,2,3,4,5-pentamethylcyclopentadienyl) with [M(CO)₅·THF] (THF = tetrahydrofuran, M = Mo and W) yielded the heterotrimetallic clusters *pileo*-[(Cp**Ru*)₂{M(CO)₃(μ -CO)(μ -H)(μ ₃-BH)B₂H₅], M = Mo (**2**), W (**3**) and the known *arachno* ruthenaboranes [1,2-(Cp**Ru*)(Cp**Ru*CO)(μ -H)B₃H₈] (**I**) and [(Cp**Ru*(CO))₂B₂H₆] (**II**). In an attempt to synthesize the Mn-analog of **2** and **3**, we performed a similar reaction of *nido*-1 with [Mn₂(CO)₁₀], which afforded the heterotrimetallic *pileo*-[(Cp**Ru*){Mn(CO)₃(μ -H)₂(μ ₃-BH)B₂H₅] (**4**) cluster along with the reported trimetallic hydrido(hydroborylene) species [(Cp**Ru*)₂{Mn(CO)₃(μ -H)(μ -CO)₃(μ -BH)}] (**III**). Ruthenaboranes **2**, **3** and **4** are isoelectronic and isostructural. The geometry of **2–4** can be viewed as a triangle face-fused square pyramidal and tetrahedral geometry, in which the apical vertex of the tetrahedron is occupied by a μ ₃-BH moiety. All of these *pileo* ruthenaborane clusters obey Mingos' fusion formalism. Clusters **2–4** were characterized using multinuclear NMR, IR spectroscopies and electrospray ionization mass spectrometry. The single-crystal X-ray diffraction studies of clusters **2** and **4** confirmed their structures. Further, density functional theory (DFT) studies of these *pileo* ruthenaboranes have been carried out to investigate the nature of bonding, fusion and electronic structures.

Keywords: cluster; heterometallic; metal-rich; pileo; ruthenaboranes



Citation: Pradhan, A.N.; Jaiswal, S.; Cordier, M.; Halet, J.-F.; Ghosh, S. Metal Rich Metallaboranes: Synthesis, Structure and Bonding of *pileo*-[(Cp**Ru*)₂M(CO)₃(μ -H)(μ -E)(μ ₃-BH)B₂H₅] (M = Mo, W, E = CO, and M = Mn, E = H) Clusters. *Inorganics* **2024**, *12*, 7. <https://doi.org/10.3390/inorganics12010007>

Academic Editor: Marius Andruh

Received: 17 November 2023

Revised: 14 December 2023

Accepted: 20 December 2023

Published: 23 December 2023



Copyright: © 2023 by the authors. Licensee MDPI, Basel, Switzerland. This article is an open access article distributed under the terms and conditions of the Creative Commons Attribution (CC BY) license (<https://creativecommons.org/licenses/by/4.0/>).

1. Introduction

In the past few decades, the study of boron cage compounds has emerged as an innovative and intriguing area of chemistry. This is due to boron's extraordinary capacity to form stable, three-dimensional clusters that are covalently bonded rather than chains and rings [1–4]. This arises from the fact that it has one less valence electron than the number of valence orbitals, and the variety of ways in which boron seeks to solve the problem of having fewer electrons than atomic orbitals available for bonding (its “electron deficiency”) results in its rich chemistry. One solution is to adopt high connectivity with many boron–boron contacts, leading to polyhedral borane compounds with some unusual bonding features and unique structural motifs to compensate for this electron deficiency. Over the years, the synthesis and characterization of such polyhedral borane clusters with single- and condensed-cage geometries have garnered a lot of attention, built on the pioneering work of Alfred Stock ninety years ago [5]. By introducing carbon, main group, or transition-metal fragments to the polyhedral skeletons, many borane, carborane, metallaborane, metallacarborane and metallaheteroborane species have been isolated and

characterized [6–12]. These species often demonstrate intriguing properties apart from their peculiar three-dimensional geometries and typical multicenter bonding interactions [13–15]. Some of them have been utilized in supramolecular design, ceramics, medicines, catalysis, nanomaterials, and polymer chemistry, for instance [16–27]. In parallel to the polyhedral clusters, another class of TM boron complexes with low boron content is of interest [2,8]. In particular, following the pioneering work of several people such as Fehlner [4,28], Kennedy [6,29] or Housecroft [11,30,31], to mention a few, we have contributed to enriching the library of the metal-rich single-cage and condensed-cage polyhedral clusters of early and late transition metals (TMs) over the last two decades [8].

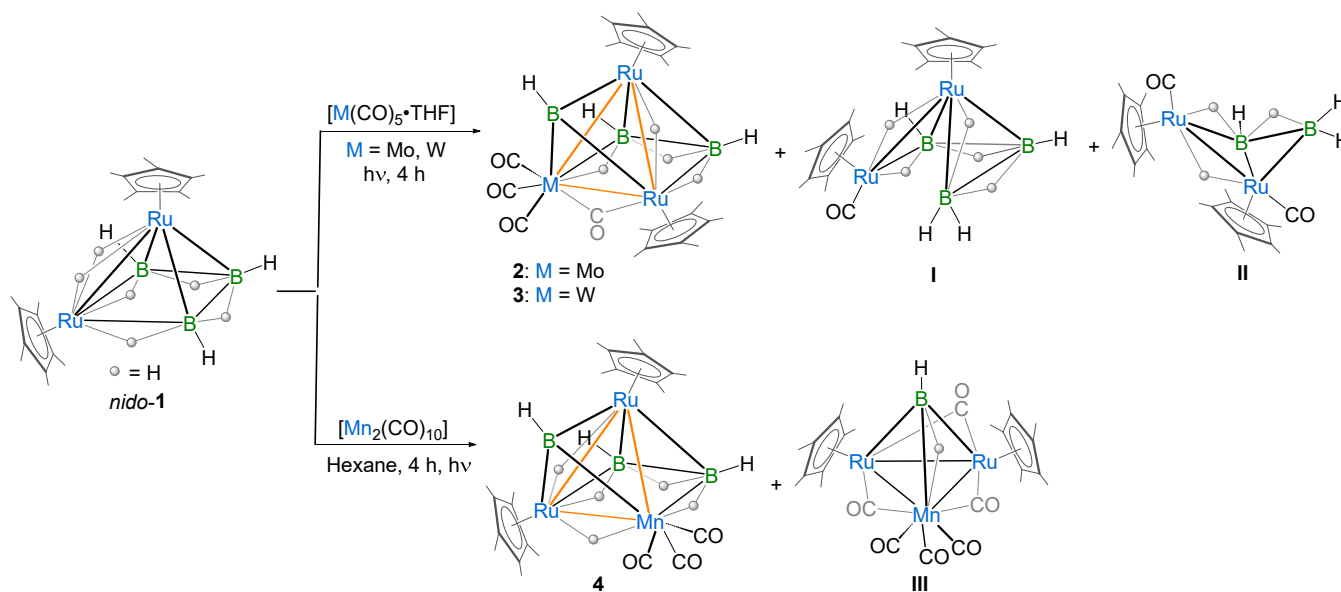
The electron-counting principles that Wade and Williams [32–35] first proposed for single-cage boranes and were further developed by Mingos [36] and Jemmis [37,38] for single and fused polyhedral cages and their metal or main group derivatives have proven helpful for classifying and rationalizing the structural and electronic properties of these clusters, connecting the number of vertices n of the cage and the number of skeletal electron pairs (SEPs) [39,40]. Additionally, these electron-counting rules were useful for establishing new classes of closed and open polyhedral clusters and, depending on the number of missing vertices in the pseudo-deltahedral geometry, they were classified as *closo* ($n + 1$ SEP), *nido* ($n + 2$ SEPs), or *arachno* ($n + 3$ SEPs). Although thousands of such compounds have been synthesized, examples of clusters with capping vertices are not very common. The clusters with *pileo* geometry have a dual role. First, they describe systems with n SEPs. Second, they describe corresponding n -vertex clusters with a capped closed polyhedral [41]. Some of the known examples are *pileo*-[(PPh₃)₃(CO)₂OsB₅H₅IrH] [42,43], *pileo*-[(CpFe)(ML₃H)B₅H₇], and (M = Mo, L = PMe₂Ph, M = W, L = PMe₃) [44], reported by Barton's and Green's groups, respectively. For such hydride species where several geometric isomers are possible for a given number of SEPs, the observed isomeric form will depend on the steric and electronic demands of the bridging hydrogens, which contribute significantly to the energetics of these species. The specific role of bridging and extra skeletal hydrogens in cage bonding can give rise to specifications for their arrangement within the electron counting rules. Essentially, polyhedral metallaboranes can be viewed as a molecular bridge connecting polyhedral borane cages with transition metal clusters. This is a result of the Hoffmann's isolobal principle, which states that a transition metal fragment can be considered to be isolobal with a BH unit or any monosubstituted boron center making up polyhedral boron clusters, and may consequently play an important role in cluster bonding [45].

As part of our research on such clusters, we performed the reaction of preformed metallaboranes with metal carbonyls in different conditions such as room temperature and heating [8,46,47]. Using this synthetic strategy, we have isolated and synthesized a series of metal-rich single- and condensed-cage metallaboranes in recent years. The reaction of ruthenaboranes, e.g., *nido*-[(Cp*Ru)₂(μ-H)₂B₃H₇] (*nido*-1) [48] and *arachno*-[(Cp*Ru(CO))₂B₂H₆] (**II**) [46], with different metal carbonyls afforded metal-rich triply bridged borylenes, interstitial and semi-interstitial borides and condensed clusters [8,46,47]. Very recently, we reported the formation of heterometallic metal-rich clusters from the reaction of *nido*-1 with group 7 metal carbonyls [M₂(CO)₁₀] (M = Mn, Re). The photolytic reaction afforded the hydrido(hydroborylene) compounds [(Cp*Ru)₂M(CO)₃-(μ-H)(μ-CO)₃(μ-BH)] (M = Mn, Re), the heterotrimetallic square pyramidal cluster [(Cp*Ru)₂Re(CO)₃(μ-H)₂(μ-CO)(μ,η²-B₂H₅)] and the planar heterotrimetallic hydride clusters [Cp*Ru(CO)_x{Re(CO)₄}(μ-H)_y] ($x = 2, y = 1$ and $x = 1, y = 3$) [49]. Herein, we describe the synthesis, structure and bonding of *pileo*-[(Cp*Ru)₂M(CO)₃(μ-H)(μ-E)(μ₃-BH)B₂H₅] (M = Mo, W, E = CO, and M = Mn, E = H) clusters.

2. Results and Discussion

*Synthesis of the Pileo-Heterotrimetallic Clusters [(Cp*Ru)₂M(CO)₃(μ-H)(μ-E)(μ₃-BH)B₂H₅] (M = Mo, W, E = CO, and M = Mn, E = H)*

In recent years, we have reported the formation of heterometallic metal-rich clusters of early and late TMs [8,46,47]. In the past, all of these reactions were carried out under thermolytic conditions or at room temperature. Interestingly, in the photolytic conditions, we performed a reaction that led to the formation of a series of metal-rich metallaboranes [49]. So, relying on these results, we explored the chemistry with group 6 and 7 metal carbonyls. In an attempt to isolate similar types of heterometallic metal-rich clusters, we performed the room temperature photolytic reaction of *nido*-[(Cp*Ru)₂(μ-H)₂B₃H₇] (*nido*-1) with [M(CO)₅·THF] (M = Mo and W) for 4 h, which led to the formation of *pileo*-[(Cp*Ru)₂{M(CO)₃(μ-CO)(μ-H)(μ₃-BH)B₂H₅], [M = Mo (2) *R_f* = 0.52 in CH₂Cl₂/*n*-hexane (10:90 *v/v*) and W (3) *R_f* = 0.44 in CH₂Cl₂/*n*-hexane (10:90 *v/v*)] and known *arachno*-[1,2-(Cp*Ru)(Cp*RuCO)(μ-H)B₃H₈] (I) [50] and *arachno*-[(Cp*Ru(CO))₂B₂H₆] (II) [46] (Scheme 1). In an attempt to synthesize the Mn-analog of 2 and 3, we carried out the room temperature photolytic reaction of *nido*-1 with [Mn₂(CO)₁₀] in hexane for 4 h, which led to the formation of *pileo*-[(Cp*Ru)₂Mn(CO)₃(μ-H)₂(μ₃-BH)B₂H₅] (4) [*R_f* = 0.71 in CH₂Cl₂/*n*-hexane (10:90 *v/v*)], I and the reported hydrido(hydroborylene) [(Cp*Ru)₂{Mn(CO)₃(μ-H)(μ-CO)₃(μ-BH)}] (III) (Scheme 1). Ruthenaborane clusters 2, 3 and 4 were characterized by multinuclear NMR, IR spectroscopies and mass spectrometry. Finally, single-crystal diffraction analysis was performed to determine the structure of clusters 2 and 4.



Scheme 1. Synthesis of *pileo* heterotrimetallic clusters 2–4 and I–III.

Heterotrimetallic clusters: Clusters 2–4 were isolated in 26%, 22% and 24% yields, respectively, as air-stable orange solids. The room-temperature ¹¹B{¹H} NMR spectra of clusters 2–4 show three distinct chemical shifts at δ = 120.7, 15.9, −0.2 (2), 122.3, 21.2, 0.4 (3) and 118.0, 21.9, −1.5 (4) ppm in a 1:1:1 ratio. The downfield broad chemical shifts at δ = 120.7, 122.3 and 118.0 ppm, for 2–4, respectively, indicate the presence of a bridging borylene boron atom. The presence of a borylene moiety is also confirmed by the broad peaks at δ = 8.71, 9.31 and 8.59 ppm in the ¹H NMR spectra of 2, 3 and 4, respectively, which are the characteristic peaks of a borylene moiety. Further, clusters 2, 3 and 4 exhibit a sharp peak at δ = −12.89, −12.52 and −12.13 ppm, respectively, which may be due to the presence of ruthenium hydrides. The ¹H spectra of 2–4 indicate the presence of two different Cp* environments, which was further validated by the ¹³C{¹H} NMR spectra of 2 and 3. In addition, the ¹H spectra display broad upfield resonances at δ = −3.64, −10.37, −15.06 (2), −3.91, −11.55, −14.37 (3) and −3.98, −15.13 (4) ppm that may be due to B-H-B,

M-H-B (M = Mo, W and Mn) or Ru-H-B. In **4**, the upfield sharp signals at $\delta = -17.97$ ppm correspond to Mn-H-Ru.

The IR spectra exhibit bands for terminal BH, terminal and bridging CO ligands of clusters **2** and **3**, whereas cluster **4** shows peaks for only terminal BH and terminal CO ligands. The ESI-MS spectra of clusters **2–4** show isotopic patterns at $m/z = 720.0142$, 810.0559 and 653.0523 that correspond to $C_{23}H_{38}O_4B_3Ru_2Mo [M]^+$, $C_{23}H_{39}O_4B_3Ru_2W [M + H]^+$, and $C_{23}H_{38}O_4B_3Ru_2Mn [M]^+$, respectively. Although the broad resonances in 1H and $^{11}B\{^1H\}$ suggest the presence of a borylene species (μ -BH), their exact core geometries were not anticipated from these spectroscopic data. In order to interpret the structures and to confirm the spectroscopic assignments, a single-crystal X-ray diffraction study was performed on crystals from **2** and **4**.

Suitable crystals for X-ray diffraction were obtained from the hexane/ CH_2Cl_2 solution of clusters **2** and **4** at 5 °C. Both clusters **2** and **4** crystallize in the monoclinic system with space group $P2_1/n$. As shown in Figure 1, clusters **2** and **4** can be considered as adopting a *nido*-square pyramidal geometry capped by a BH fragment. The geometry of cluster **3** was established through the comparison of its spectroscopic data with cluster **2** and other similar *pileo*-trimetallic metallaboranes (Table 1) [47,51,52]. The structure of **3** seems similar to **2**, and can also be considered as having a capped *nido*-square pyramidal Ru_2MB_3 (M = Mo, W) geometry. Alternatively, the core geometry of these clusters can also be viewed as a face-fused polyhedron composed of an Ru_2MB_2 (M = Mo, W, Mn) distorted square pyramid and an $RuMB$ (M = Mo, W, Mn) tetrahedral framework (Figure 2). This kind of cluster can be referred to as a *pileo* structure with a monocapped square pyramidal geometry analogous to that of pentaborane(9). One interesting feature of clusters **2–4** is the presence of a bridging borylene ligand (μ_3 -BH). The generation of clusters **2–4** can be described by the geometry rearrangement of *nido*-**1**. One BH moiety might be replaced from the basal position to the capped position to produce clusters **2** and **3** by introducing one $\{M(CO)_3\}$ fragment and a bridging CO ligand in the basal position, followed by the elimination of a H_2 unit. However, in **4**, there is no bridging CO ligand between Ru and Mn to satisfy the electron count. Three *endo* hydrogens and one CO in **2** and **3** bridge the distorted open square face $[Ru_2MB_2]$ (M = Mo, W) and one hydrogen bridges two Ru atoms, whereas in **4**, four *endo* hydrogens bridge the distorted open square face $[RuMnB_2]$. Similar to clusters **2** and **3**, one hydrogen bridges one apical and one basal Ru atom in **4**. The distorted square pyramidal core of **2–4** is similar to that encountered in $[(Cp^*Ru)_2\{Re(CO)_3\}(\mu-H)_2(\mu-CO)B_2H_5]$ [49] and $[\{Ru(CO)_3\}_3(\mu-H)B_2H_5]$ [53,54]. The existence of clusters **2–4** allows us to draw a structural comparison with the reported clusters with a similar geometry, but with different transition metals (Table 1) [47,51,52]. The axial Ru atom of the distorted square pyramid is situated approximately 1.804 Å (**2**) and 1.784 Å (**4**) above the $RuMB_2$ square plane, which is comparable to distances measured in the similar types of clusters shown in Table 1. The two ruthenium atoms (apical and basal) are separated by an intermetallic distance of 2.7738(3) Å (**2**) and 2.7536(5) Å (**4**), which is in the typical range for a Ru-Ru single bond, but less compared to distances in homometallic *pileo*- $[(Cp^*Ru)_3(\mu-H)_2(\mu_3-BX)B_2H_5]$ (X = H (2.807 Å) [51], Cl (2.8323 Å) [47]. In addition, the observed B-B bond distances of 1.796(3) Å (**2**) and 1.781(8) Å (**4**) suggest the presence of B-B single bonds in **2** and **4** and comparatively less than in the similar clusters reported in Table 1 [47,51,52]. The core geometry of **2–4** is also comparable to the homo- and heterometallic clusters *pileo*-2,3- $[\{Fe(PMe_3)_2\}_2(\mu-H)B_4H_9]$ [55], *pileo*-2,3- $[(Cp^*Ru)_2(\mu-H)B_4H_7]$ [48], *pileo*- $[(Cp^*Rh)\{Ru(CO)_3\}_4(\mu-Cl)B]$ [56], *pileo*- $[(Cp^*TaCl)\{Ru_3(CO)_8\}(\mu-Cl)B_2H_4]$ [8], different geometrical isomers of *pileo*-2,3- $[(Cp^*Ru)_2(\mu-H)B_4H_5Cl_2]$ and *pileo*-2,3- $[(Cp^*Ru)_2(\mu-H)B_4H_4Cl_4]$ [57]. The average Ru-B bond length in **4** (2.170 Å) is comparable with that in *pileo*- $[(Cp^*Ru)_3(\mu-H)_2(\mu_3-BX)B_2H_5]$ (X = H [51], Cl [47], whereas this bond length is longer in the case of **2** (2.320 Å). As shown in Figure 1, the orientations of the $\{Mo(CO)_3\}$ and $\{Mn(CO)_3\}$ fragments are different in **2** and **4**. The orientation in **2** is similar to *pileo*- $[(Cp^*Rh)_2\{Cr(CO)_3\}(\mu-CO)(\mu_3-BH)B_2H_4]$ [47], whereas in **4**, it is similar to that in *pileo*- $[(Cp^*Rh)_2\{M(CO)_3\}(\mu-CO)(\mu_3-BH)B_2H_4]$ (M = Mo, W) [52]. In **2**, the average Mo-B (2.383 Å)

and Ru-Mo (2.849 Å) bond lengths are in accordance with those reported in molybdaboranes [52,58]. Also, the average Mn-Ru (2.768 Å) and Mn-B (2.236 Å) bond distances in **4** are in the range of those reported for the related clusters [59,60]. The qualitative shape of clusters **2** and **4** is similar and the only significant geometrical difference is the slight deviation of the dihedral angle between Ru_2M' and RuB_2 planes from 114.6° (**2**) to 115.9° (**4**) upon moving from group 6 to 7 (Figure 2). The corresponding dihedral angle between the planes M_2M' and MB_2 in the reported *pileo*-trimetallic metallaboranes ranges from 114 to 119° (Table 1).

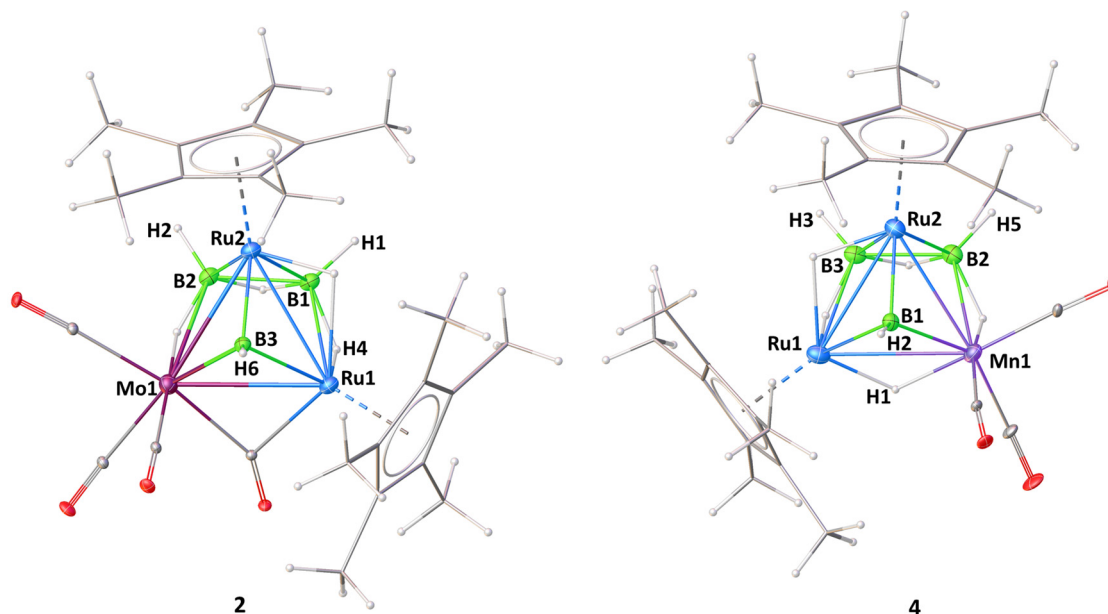


Figure 1. Molecular structures and labeling diagrams of **2** (left) and **4** (right). Selected bond lengths (Å) and bond angles ($^\circ$); **2**: Ru1-B1 2.410(2), Ru1-B3 2.218(2), Ru2-B2 2.172(2), Ru1-Ru2 2.7738(3), Ru1-Mo1 2.8589(3), Ru2-Mo1 2.8395(3), Mo1-B3 2.265(2), Mo1-B2 2.501(2), B1-B2 1.796(3), Ru1-B3-Mo1 79.22(7), B2-B1-Ru1 104.17(13), B1-Ru2-B2 49.02(9), B1-Ru1-Ru2 48.59(5); **4**: B1-Ru2 2.008(5), B1-Mn1 2.154(5), B2-Mn1 2.318(6), B1-Ru1 2.176(5), B2-B3 1.781(8), B2-Ru2 2.133(5), B3-Ru2 2.152(5), Mn1-Ru2 2.7096(8), Mn1-Ru1 2.8280(8), Ru1-Ru2 2.7536(5), Mn1-B1-Ru1 81.55(16), B3-B2-Mn1 102.6(3), Ru2-B2-Mn1 74.85(16), Ru2-B3-Ru1 74.41(14), B2-Mn1-Ru2 49.47(12).

Table 1. Selected spectroscopic and structural parameters of *pileo*-trimetallic metallaboranes.

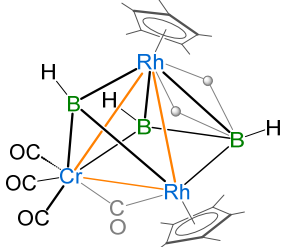
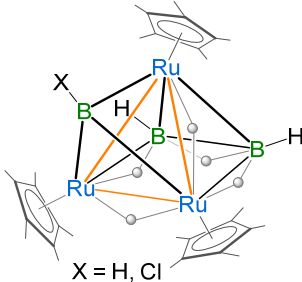
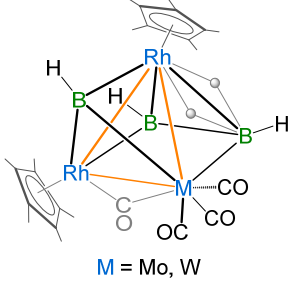
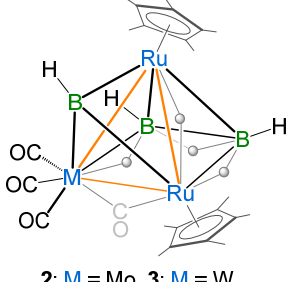
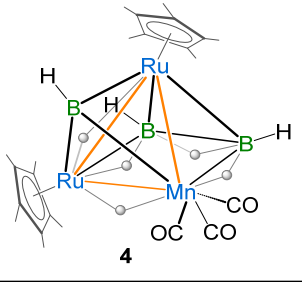
Clusters	$d(B-B)_{av}$ (Å)	Dihedral Angle $^\circ$ b	$d(\Pi MM'B_2-M)^a$ (Å)	^{11}B NMR (δ , ppm)	Ref.
	1.82 (3)	117.6	1.748	121.3, 59.9, 23.5	[47]

Table 1. Cont.

Clusters	$d(\text{B-B})_{\text{av}}$ (Å)	Dihedral Angle ($^{\circ}$) b	$d(\text{IIMM}'\text{B}_2\text{-M})^a$ (Å)	^{11}B NMR (δ , ppm)	Ref.
 X = H, Cl	1.874 (11) (H) 1.806 (6) (Cl)	119.2 (H) 117.9 (Cl)	1.821 (H) 1.807 (Cl)	128.3, 14.4 (H) 114.5, 32.6, −0.9 (Cl)	[51] [47]
 M = Mo, W	1.814 (19) (Mo) 1.829 (16) (W)	116.7 (Mo) 116.7 (W)	1.778 (Mo) 1.771 (W)	124.8, 60.7, 20.1 (Mo) 126.0, 59.9, 22.5 (W)	[52]
 2: M = Mo, 3: M = W	1.796 (3) (Mo) — (W)	114.6 (Mo) — (W)	1.804 (Mo) — (W)	120.6, 15.9, −0.2 (Mo) 122.3; 21.2, 0.4 (W)	this work
 4	1.781 (8)	115.9	1.784	118.0, 21.9, −1.5	this work

^a M = Cp*Rh, Cp*Ru, M' = Cp*Ru, Cr/Mo/W/Mn(CO)₃, ^b angle between planes Ru₂M and RuB₂, av = average, d = distance.

A series of metal-rich metallaboranes with a condensed geometry is documented in the literature with different structural motifs of borons and metals. As discussed earlier, Wade, Mingos, Jemmis, and others proposed various complementary electron-counting rules for rationalizing the geometries of the main group and TM condensed clusters with respect to their cluster valence electron count (cve) and skeletal electron pairs (SEPs) [32–38]. According to polyhedral skeletal electron pair theory (PSEPT) [36], clusters 2–4 share the same skeleton electron pairs (7 SEPs), i.e., (n + 1) (2, 3: 2Cp*Ru (2 × 1 = 2) + 3BH (3 × 2 = 6) + 4H (4) + Mo(CO)₃/W(CO)₃ (0) + CO (2) = 14 electrons = 7 SEPs), 4: 2Cp*Ru (2 × 1 = 2) + 3BH (3 × 2 = 6) + 5H (5) + Mn(CO)₃ (1) = 14 electrons = 7 SEPs) as that of *nido-1*, despite having *pileo* geometry. The electron count for clusters 2–4 was justified using Mingos' fusion formalism, which is equal to the electron count for the parent cluster minus the electron count of shared units. Thus, the total cve count accessible for 2–4 is 56 {square

pyramid $[\text{Ru}_2\text{MB}_2]$ (54 e) + tetrahedron $[\text{Ru}_2\text{MB}_2]$ (50 e)—triangle $[\text{Ru}_2\text{M}]$ (48 e) = 56 e), which is the same if one uses the fused polyhedral model (2, 3: $2\text{Cp}^*\text{Ru}$ ($2 \times 13 = 26$) + 3B ($3 \times 3 = 9$) + 7H (7) + M (6) + 4CO ($4 \times 2 = 8$) = 56 e, 4: $2\text{Cp}^*\text{Ru}$ ($2 \times 13 = 26$) + 3B ($3 \times 3 = 9$) + 8H (8) + Mn (7) + 3CO ($3 \times 2 = 6$) = 56 e).

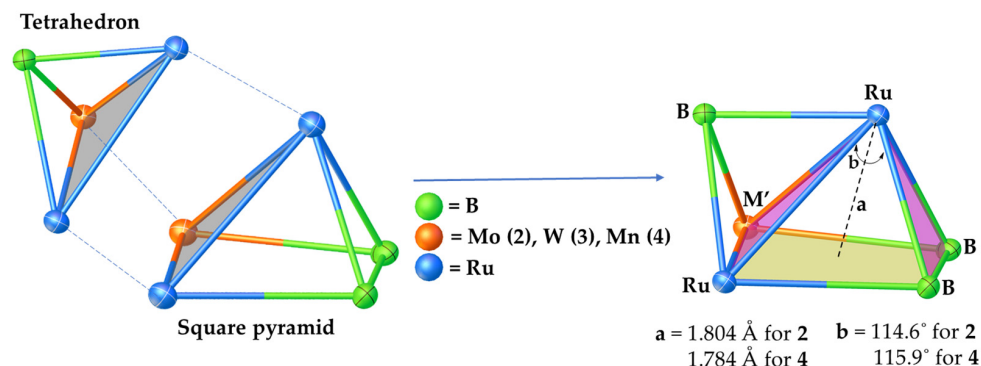


Figure 2. Schematic representation of the cluster fusion in clusters 2–4 (a = distance of apical Ru from square plane RuMB_2 , b = dihedral angle between planes $\text{Ru}_2\text{M}'$ and RuB_2).

Density functional theory (DFT) calculations were performed at the BP86/def2-TZVP level of theory on clusters 2, 3 and 4 to gain some insights into their bonding and electronic properties. The molecular orbital analyses of 2 (Figure 3a), 3 (Figure 3c) and 4 (Figure 3e), indicate that the HOMOs are essentially localized on the metal atoms. In cluster 4, there is also some presence of a weak bonding interaction involving the H $1s$ orbital and d orbitals of Ru1 and Mn1 centers. Further, the LUMO of 2 (Figure 3b), 3 (Figure S17e) and 4 (Figure S18e) display antibonding interactions between the metal atoms (Ru, Mo for 2, Ru, W for 3 and Ru, Mn for 4). Additionally, HOMO-9 of 2 (Figure S16c), 3 (Figure 3d) and 4 (Figure 3f) shows strong bonding interaction between the capped boron atom and the Ru_2M triangle, which suggests a μ_3 -bonding mode for the boron atom. Let us note that HOMO-12 and HOMO-13 in 4 show extended overlap involving metal d -orbitals and boron p -orbitals, as shown in Figures 4a and S18c (not shown in the case of clusters 2 and 3).

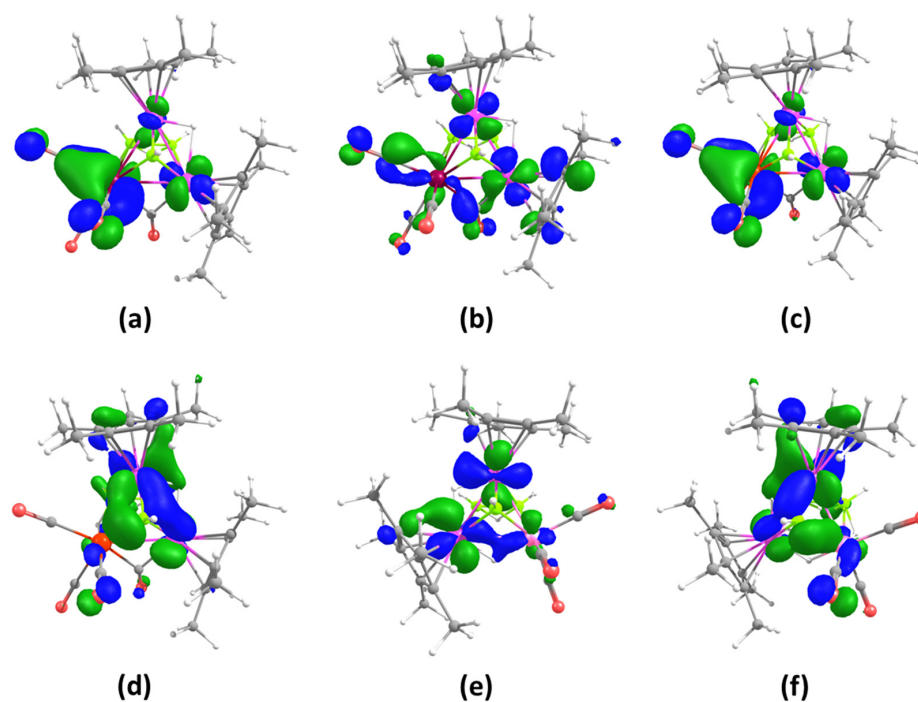


Figure 3. Selected molecular orbitals of 2–4: (a) HOMO of 2, (b) LUMO of 2, (c) HOMO of 3, (d) HOMO-9 of 3, (e) HOMO of 4, (f) HOMO-9 of 4. Isocontour values: ± 0.04 [$\text{e}\cdot\text{bohr}^{-3}$] $^{1/2}$.

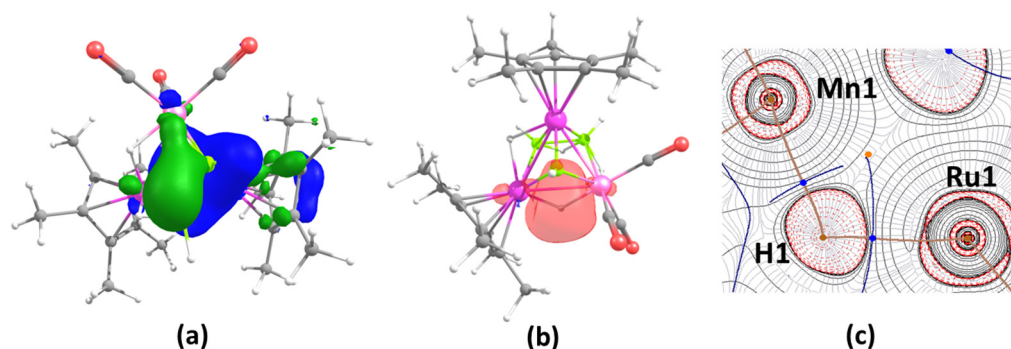


Figure 4. (a) HOMO-13 of **4** (isocontour values: ± 0.04 [e.bohr $^{-3}$] $^{1/2}$), (b) selected NBO of **4**, (c) contour line diagram of the Laplacian electron density in the Ru1-H1-Mn1 plane. Solid red lines illustrate areas of charge concentration [$(\nabla^2\rho(r) < 0)$] in the contour line diagrams of the Laplacian electron density, whereas dashed black lines show areas of charge depletion [$(\nabla^2\rho(r) > 0)$]. Bond-critical points (BCPs) are shown with blue dots, while bond routes are shown with a brown line.

A Natural Bond Orbital (NBO) analysis indicated the existence of a three-center-two-electron bond along the Ru1-H1-Mn1 in **4** (Figure 4b). This was further confirmed from a topological analysis showing that the contour line map displays bond-critical points (BCPs) between Ru1-H1 and Mn1-H1 bonds in the Ru1-H1-Mn1 plane, as depicted in Figure 4c. Surprisingly, the NBO analysis unexpectedly revealed that the capped boron atom has a very high positive natural charge in the case of clusters **2–4** (0.74, 0.68 and 0.72 for **2**, **3** and **4**, respectively), while the other two planar boron atoms possess small negative natural charges (-0.11 and -0.10 for **2**, -0.13 and -0.10 for **3**, and -0.06 and -0.10 for **4**), as shown in Table S2, indicating that the capped boron should be very prone to nucleophilicity.

3. Materials and Methods

3.1. General Methods and Instrumentation

All of the reactions were accomplished under an argon atmosphere with standard Schlenk line and glove box techniques. All of the solvents were distilled using appropriate drying agents prior to use. CDCl_3 was degassed and distilled before recording all NMR spectra and stored over molecular sieves. *Nido*-1,2-[(Cp* RuH) $_2\text{B}_3\text{H}_7$] (*nido*-**1**) [48] was prepared according to literature methods, while $[\text{LiBH}_4\cdot\text{THF}]$, $[\text{Mo}(\text{CO})_6]$, $[\text{W}(\text{CO})_6]$ and $[\text{Mn}_2(\text{CO})_{10}]$ were obtained commercially and used as received. Thin-layer chromatography (TLC) was performed on 250 mm aluminum-supported silica gel TLC plates. The NMR spectra were recorded on 500 MHz Bruker FT-NMR spectrometers. The residual solvent protons were used as a reference (δ , ppm, CDCl_3 , 7.26) and the residual solvent carbon for $^{13}\text{C}\{^1\text{H}\}$ NMR spectra was used as a reference (δ , ppm, CDCl_3 , 77.16 and δ , ppm, d_6 -benzene, 128.07). A sealed tube containing $[\text{Bu}_4\text{N}(\text{B}_3\text{H}_8)]$ (δ_{B} , -30.07 ppm) in C_6D_6 was used as external reference in ^{11}B NMR, which was synthesized according to the method in the literature [61]. The ^{11}B -decoupled ^1H spectra were obtained with inverse gated decoupling (zgig) pulse sequences. All pulse sequences are available in a commercial Bruker spectrometer. ^1H -decoupled ^{11}B spectra were processed with a backward linear prediction algorithm to remove the broad ^{11}B background signal from the NMR probe and NMR tube [62,63]. The ESI-MS spectra were recorded on 6545 Qtof LC/MS and Qtof Micro YA263 HRMS instruments. The IR spectra were recorded on a JASCO FT/IR-1400 apparatus using a dichloromethane (CH_2Cl_2) solvent. The photoreactions described here were conducted in an LZC-4 V Luzchem photoreactor (Luzchem Research, Inc., Gloucester, ON, Canada) with 14 UVA lamps (8 W HITACHI FL8BL-B; $\lambda = (350 \pm 50)$ nm).

Synthesis of 2 and 3: In a flame-dried Schlenk tube, a yellow solution of *nido*-**1** (0.1 g, 0.19 mmol) was taken and a freshly prepared yellow solution of $[\text{Mo}(\text{CO})_5\cdot\text{THF}]$ (UV irradiation of $\text{Mo}(\text{CO})_6$ (0.07 g) in 10 mL of THF for 20 min) was added dropwise using a cannula at ambient temperature. The reaction mixture was UV-irradiated for over 4 h and the color change from yellow to red was observed. The solution was subjected to

evaporation under reduced pressure and subjected to thin-layer chromatography using silica gel TLC plates for the separation of the reaction mixture. Elution with CH₂Cl₂/hexane (10:90 *v/v*) yielded air-stable pure orange solid **2** (0.037 g, 26%) and known yellow **I** (0.019 g, 19%) [50] and **II** (0.009 g, 7%) [46]. Note that the treatment of *nido-1* with [W(CO)₅·THF] (UV irradiation of W(CO)₆ (0.07 g) in 10 mL of THF for 20 min) afforded orange **3** (0.035 g, 22%) along with clusters **I** (0.019 g, 19%) and **II** (0.009 g, 7%).

2: MS (ESI+) calcd. for C₂₃H₃₈O₄B₃Ru₂Mo [M]⁺ *m/z* 720.0155, found 720.0142; ¹¹B NMR (22 °C, 128 MHz, CDCl₃): δ = 120.7, 15.9, −0.2 ppm; ¹H NMR (22 °C, 500 MHz, CDCl₃): δ = 3.42 (br, 1H, BH_t), 4.62 (br, 1H, BH_t), 8.71 (br, 1H, BH_t), 1.92 (s, 15H, Cp*), 1.79 (s, 15H, Cp*), −3.64 (1H, B-H-B), −10.37 (1H, Ru-H-B), −12.89 (1H, Ru-H-Ru), −15.06 (1H, Mo-H-B) ppm; ¹³C{¹H} NMR (22 °C, 100 MHz, CDCl₃): δ = 10.4, 11.0 (s, C₅Me₅), 98.7 (s, C₅Me₅) (accidental overlapping of two Cp* ligands's chemical shifts), 251.2 (CO) ppm; IR (CH₂Cl₂, cm^{−1}): 2489, 2455 (BH_t), 1994, 1933, 1875 (terminal CO), 1788 (bridging CO).

3: MS (ESI+) calcd. for C₂₃H₃₉O₄B₃Ru₂W [M + H]⁺ *m/z* 810.0695, found 810.0559; ¹¹B NMR (22 °C, 128 MHz, CDCl₃): δ = 122.3; 21.2, 0.4 ppm; ¹H NMR (22 °C, 500 MHz, CDCl₃): δ = 3.46 (br, 1H, BH_t), 4.12 (br, 1H, BH_t), 9.31 (br, 1H, BH_t), 1.78 (s, 15H, Cp*), 1.93 (s, 15H, Cp*), −3.91 (1H, B-H-B), −11.55 (1H, Ru-H-B), −12.52 (1H, Ru-H-Ru), −14.37 (1H, W-H-B) ppm; ¹³C{¹H} NMR (22 °C, 100 MHz, CDCl₃): δ = 10.4, 11.0 (s, C₅Me₅), 98.8, 95.8 (s, C₅Me₅) 249.4 (CO) ppm; IR (CH₂Cl₂, cm^{−1}): 2468, 2435 (BH_t), 1994, 1936, 1875 (terminal CO), 1794 (bridging CO).

Synthesis of **4**: In a flame-dried Schlenk tube, a yellow solution of *nido-1* (0.100 g, 0.19 mmol) and [Mn₂(CO)₁₀] (0.045 g, 0.11 mmol) in hexane (15 mL) was taken. Then, the mixture was UV-irradiated for over 4 h. The volatile components were removed under vacuum. After the removal of the solvent, the residue was subjected to chromatographic workup using silica gel TLC plates. Elution with CH₂Cl₂/hexane (10:90 *v/v*) yielded air-stable pure orange **4** (0.031 g, 24%) and **III** (0.008 g, 6%) [49].

4: MS (ESI+) calcd. for C₂₃H₃₈O₄B₃Ru₂Mn [M]⁺ *m/z* 653.0602, found 653.0523; ¹¹B NMR (22 °C, 128 MHz, CDCl₃): δ = 118.0, 21.9, −1.5 ppm; ¹H NMR (22 °C, 500 MHz, CDCl₃): δ = 2.32 (br, 1H, BH_t), 4.07 (br, 1H, BH_t), 8.59 (br, 1H, BH_t), 1.86 (s, 15H, Cp*), 1.93 (s, 15H, Cp*), −3.98 (1H, B-H-B), −12.13 (1H, Ru-H-Ru), −15.13 (2H, Mn-H-B, Ru-H-B), −17.97 (1H, Ru-H-Mn) ppm; IR (CH₂Cl₂, cm^{−1}): 2485, 2448 (BH_t), 2001, 1929, 1902 (terminal CO).

3.2. Single-Crystal X-ray Diffraction Analysis

The crystallographic and structural refinement data of **2** and **4** are given in Table 2. Suitable X-ray-quality crystals of **2** and **4** were grown via the slow diffusion of a *n*-hexane/CH₂Cl₂ solution at 5 °C. The crystal data were collected and integrated using a Bruker APEX-II CCD diffractometer for **2**, and Bruker APEXII CCD for **4**, with graphite monochromated Mo Kα (λ = 0.71073 Å) radiation at 296(2) K. The structures of these compounds were solved using heavy atom methods with SHELXS-97 and SHELXT-2014 [64–66] and refined with SHELXL-2014, SHELXL-2017 and SHELXL-2018 [65]. All molecular structures were drawn using Olex2 [67].

Table 2. Crystallographic and structural refinement data for **2** and **4**.

Compound	2	4
CCDC No.	2192116	2192115
Empirical formula	C ₂₄ H ₃₇ B ₃ MoO ₄ Ru ₂	C ₂₃ H ₃₈ B ₃ MnO ₃ Ru ₂
Formula weight	720.04	652.04
Crystal system	monoclinic	monoclinic
Space group	<i>P</i> 2 ₁ / <i>n</i>	<i>P</i> 2 ₁ / <i>n</i>
<i>a</i> (Å)	10.9696(12)	9.3964(13)
<i>b</i> (Å)	13.7372(17)	14.3307(17)
<i>c</i> (Å)	18.383(2)	20.306(2)
α (°)	90	90
β (°)	100.328(4)	94.870(5)

Table 2. Cont.

Compound	2	4
γ (°)	90	90
Volume (Å ³)	2725.3(5)	2724.4(6)
Z	4	4
ρ_{calc} (g/cm ⁻³)	1.755	1.590
μ (mm ⁻¹)	1.575	1.572
F (000)	1432	1312
2 θ range for data collection (°)	55.028	50
Independent reflections	6153	4792
Final R indices [$I \geq 2\sigma(I)$]	0.0226	0.0644
Parameters	338	331

3.3. Computational Details

The optimization of clusters 2–4 was carried out using the *Gaussian 16* program [68] with the BP86 functional [69,70] and the def2-TZVP basis set [71] from the EMSL (Environmental Molecular Sciences Laboratory) Basis Set Exchange Library [72]. The model compounds were thoroughly optimized without any solvent effect in the gaseous state, starting with X-ray crystallographic structures. Frequency calculations were carried out to check the nature of the stationary states and to confirm the absence of any imaginary frequency, which eventually confirmed energy minima on the potential energy hyper surface for all structures. A natural bond orbital (NBO) [73] analysis was performed with the NBO partitioning scheme implemented in the *Gaussian 16* code. The *Chemcraft* [74] visualization program was used to plot all of the optimized structures and orbital pictures. The *Multwfn* V.3.6 package [75] was used to create two-dimensional electron density and Laplacian electronic distribution plots.

4. Conclusions

In this article, we have demonstrated the isolation and structural characterization of new *pileo* heterotrimetallic clusters 2–4 in the coordination sphere of group 6, 7 and 8 transition metals. Clusters 2–4 possess a *pileo* geometry with 7 SEPs ($n + 1$). One of the interesting features of all of these clusters is the existence of a triply bridging borylene ligand (μ_3 -BH), which is stabilized by the heterotrimetallic transition metal (Ru₂M, M = Mo, W and Mn) framework. The geometry of these clusters can also be considered as the outcome of the fusion of a trimetallic tetrahedron with a square pyramid, following Mingos' fusion formalism. Furthermore, we observed that the insertion of TM carbonyl fragments can generate relatively air-stable clusters.

Supplementary Materials: The following supporting information can be downloaded at: <https://www.mdpi.com/article/10.3390/inorganics12010007/s1>, ¹H, ¹¹B{¹H}, ¹³C{¹H} NMR, IR and mass spectra (Figures S1–S14); X-ray analysis details and CIF and checkCIF files as well as the xyz coordinates of the DFT-optimized model clusters, calculated HOMO and LUMO energy levels and HOMO-LUMO gaps, selected bond parameters and their Wiberg bond indices (WBI) for clusters 2–4 (Figure S15–S21).

Author Contributions: A.N.P. and S.J. formulated and planned the experiments; A.N.P. and S.J. carried out the synthesis and spectroscopic analyses and discussed the results with S.G. and J.-F.H.; A.N.P. and S.J. organized the manuscript with guidance from S.G. and J.-F.H.; M.C. and J.-F.H. performed the X-ray analysis; and S.G. supervised the project and oversaw the project administration. All authors have read and agreed to the published version of the manuscript.

Funding: This work was supported by ERF, IIT Madras (grant no.—RF/2223/0528/CY/RFER/008224).

Data Availability Statement: Accession codes: 2192116 (2), 2192115 (4). Crystallographic data can be acquired for free from the Cambridge Crystallographic Data Centre via www.ccdc.cam.ac.uk/data_request/cif, accessed on 1 November 2023, by emailing data_request@ccdc.cam.ac.uk, or by

contacting the Cambridge Crystallographic Data Centre, 12 Union Road, Cambridge, CB2 1EZ, UK; Fax: +44-1223-336033.

Acknowledgments: A.N.P. thanks the University Grants Commission (UGC), India, and S.J. thanks the Council of Scientific & Industrial Research (CSIR), India, for the research fellowship. The Department of Chemistry, IIT Madras, is gratefully acknowledged for the X-ray support. The authors thank IIT Madras for the computational facilities. We thank Venkatachalam Ramkumar for single-crystal X-ray diffraction data analyses.

Conflicts of Interest: The authors declare no conflicts of interest.

References

1. Brown, L.D.; Lipscomb, W.N. Closo Boron Hydrides with 13 to 24 Boron Atoms. *Inorg. Chem.* **1977**, *16*, 2989–2996. [[CrossRef](#)]
2. Marder, T.B.; Lin, Z. Contemporary Metal Boron Chemistry I Borylenes, Boryls, Borane Sigma-Complexes, and Borohydrides. In *Structure and Bonding*; Springer: Berlin, Germany, 2008; Volume 130.
3. Shameema, O.; Pathak, B.; Jemmis, E.D. Theoretical study of the reaction of B₂₀H₁₆ with MeCN: Closo/closo to closo/nido conversion. *Inorg. Chem.* **2008**, *47*, 4375–4382. [[CrossRef](#)] [[PubMed](#)]
4. Fehlnner, T.P.; Halet, J.-F.; Saillard, J.-Y. *Molecular Clusters. A Bridge to Solid-State Chemistry*; University Press: Cambridge, UK, 2007.
5. Stock, A. *Hydrides of Boron and Silicon*; Cornell University Press: Ithaca, NY, USA, 1933.
6. Kennedy, J.D. The Polyhedral Metallaboranes. *Prog. Inorg. Chem.* **1986**, *34*, 211–434.
7. Grimes, R.N. *Carboranes*, 3rd ed.; Elsevier: Oxford, UK, 2016.
8. Kar, S.; Pradhan, A.N.; Ghosh, S. Polyhedral Metallaboranes and Metallacarboranes. In *Comprehensive Organometallic Chemistry IV*; Parkin, G., Meyer, K., O'hare, D., Eds.; Elsevier: Amsterdam, The Netherlands, 2022; Volume 9, pp. 263–369.
9. Avdeeva, V.V.; Malinina, E.A.; Kuznetsov, N.T. Boron cluster anions and their derivatives in complexation reactions. *Coord. Chem. Rev.* **2022**, *469*, 214636–214744. [[CrossRef](#)]
10. Grimes, R.N. Transition metal Metallacarboranes. In *Comprehensive Organometallic Chemistry II*; Abel, E.W., Stone, F.G.A., Wilkinson, G., Eds.; Pergamon: Oxford, UK, 1995; Volume 1, pp. 373–430.
11. Housecroft, C.E. Boron Atoms in Transition Metal Clusters. *Adv. Organomet. Chem.* **1991**, *33*, 1–50.
12. Hosmane, N.S.; Maguire, J.A. Metallacarboranes of d- and f-block metals. In *Comprehensive Organometallic Chemistry III*; Crabtree, R.H., Mingos, D.M.P., Eds.; Elsevier: Amsterdam, The Netherlands, 2007; Volume 3, pp. 175–264.
13. King, R.B. Three-Dimensional Aromaticity in Polyhedral Boranes and Related Molecules. *Chem. Rev.* **2001**, *101*, 1119–1152. [[CrossRef](#)] [[PubMed](#)]
14. Jemmis, E.D. Overlap control and stability of polyhedral molecules. *closo*-Carboranes. *J. Am. Chem. Soc.* **1982**, *104*, 7017–7020. [[CrossRef](#)]
15. Mingos, D.M.P.; Wales, D.J. *Introduction to Cluster Chemistry*; Prentice Hall: Hoboken, NJ, USA, 1990.
16. Tietze, L.F.; Griesbach, U.; Bothe, U.; Nakamura, H.; Yamamoto, Y. Novel Carboranes with a DNA Binding Unit for the Treatment of Cancer by Boron Neutron Capture Therapy. *Chem. Bio. Chem.* **2002**, *3*, 219–225. [[CrossRef](#)]
17. Hosmane, N.S.; Eagling, R.D. *Hand Book of Boron Science with Applications in Organometallics, Catalysis, Materials and Medicine*; World Scientific: Singapore, 2018.
18. Zhang, X.; Yan, H. Transition metal-induced B–H functionalization of o-carborane. *Coord. Chem. Rev.* **2019**, *378*, 466–482. [[CrossRef](#)]
19. Zhang, J.; Xie, Z. Synthesis, Structure, and Reactivity of 13- and 14-Vertex Carboranes. *Acc. Chem. Res.* **2014**, *47*, 1623–1633. [[CrossRef](#)]
20. Deng, L.; Xie, Z. Advances in the chemistry of carboranes and metallacarboranes with more than 12 vertices. *Coord. Chem. Rev.* **2007**, *251*, 2452–2476. [[CrossRef](#)]
21. Chen, M.; Zhao, D.; Xu, J.; Li, C.; Lu, C.; Yan, H. Electrooxidative B–H Functionalization of *nido*-Carboranes. *Angew. Chem. Int. Ed.* **2021**, *60*, 7838–7844. [[CrossRef](#)] [[PubMed](#)]
22. Farràs, P.; Juárez-Pérez, E.J.; Lepšík, M.; Luque, R.; Núñez, R.; Teixidor, F. Metallacarboranes and Their Interactions: Theoretical Insights and Their Applicability. *Chem. Soc. Rev.* **2012**, *41*, 3445–3463. [[CrossRef](#)] [[PubMed](#)]
23. Núñez, R.; Tarrés, M.; Ferrer-Ugalde, A.; de Biani, F.F.; Teixidor, F. Electrochemistry and Photoluminescence of Icosahedral Carboranes, Boranes, Metallacarboranes, and Their Derivatives. *Chem. Rev.* **2016**, *116*, 14307–14378. [[CrossRef](#)] [[PubMed](#)]
24. Teixidor, F.; Núñez, R.; Flores, M.A.; Demonceau, A.; Viñas, C. Forced Exo-*Nido* Rhoda and Ruthenacarboranes as Catalyst Precursors. A review. *J. Organomet. Chem.* **2000**, *614–615*, 48–56. [[CrossRef](#)]
25. Núñez, R.; Romero, I.; Teixidor, F.; Viñas, C. Icosahedral boron clusters: A perfect tool for the enhancement of polymer features. *Chem. Soc. Rev.* **2016**, *45*, 5147–5173. [[CrossRef](#)] [[PubMed](#)]
26. Kirlikovali, K.O.; Axtell, J.A.; Gonzalez, A.; Phung, A.C.; Khan, S.I.; Spokoyny, A.M. Luminescent metal complexes featuring photophysically innocent boron cluster ligands. *Chem. Sci.* **2016**, *7*, 5132–5138. [[CrossRef](#)]
27. Fink, K.; Uchman, M. Boron cluster compounds as new chemical leads for antimicrobial therapy. *Coord. Chem. Rev.* **2021**, *431*, 213684–213693. [[CrossRef](#)]

28. Ghosh, S.; Noll, B.C.; Fehlner, T.P. Expansion of iridaborane clusters by addition of monoborane. Novel metallaboranes and mechanistic detail. *Dalton Trans.* **2008**, 371–378. [[CrossRef](#)]
29. Kennedy, J.D. Macropolyhedral metallaboranes—Aspects of preparation, constitution and structure. *Coord. Chem. Rev.* **2016**, *323*, 71–86. [[CrossRef](#)]
30. Housecroft, C.E. *Boranes and Metallaboranes Structure, Bonding and Reactivity*, 2nd ed. Ellis Horwood: Frederick, MD, USA, 1994.
31. Housecroft, C.E. From metallaboranes to transition metal borides: The chemistry of metal-rich metallaborane clusters. *Polyhedron* **1987**, *6*, 1935–1958. [[CrossRef](#)]
32. Wade, K. The structural significance of the number of skeletal bonding electron-pairs in carboranes, the higher boranes and borane anions, and various transition-metal carbonyl cluster compounds. *J. Chem. Soc. D* **1971**, 792–793. [[CrossRef](#)]
33. Wade, K. Skeletal electron counting in cluster species. Some generalisations and predictions. *Inorg. Nucl. Chem. Lett.* **1972**, *8*, 559–562. [[CrossRef](#)]
34. Wade, K. Structural and Bonding Patterns in Cluster Chemistry. *Adv. Inorg. Chem. Radiochem.* **1976**, *18*, 1–66.
35. Williams, R.E. Carboranes and boranes; polyhedra and polyhedral fragment. *Inorg. Chem.* **1971**, *10*, 210–214. [[CrossRef](#)]
36. Mingos, D.M.P. Polyhedral skeletal electron pair approach. *Acc. Chem. Res.* **1984**, *17*, 311–319. [[CrossRef](#)]
37. Jemmis, E.D.; Balakrishnarajan, M.M.; Pancharatna, P.D. Unifying Electron-Counting Rule for Macropolyhedral Boranes, Metallaboranes, and Metallocenes. *J. Am. Chem. Soc.* **2001**, *123*, 4313–4323. [[CrossRef](#)]
38. Jemmis, E.D.; Balakrishnarajan, M.M.; Pancharatna, P.D. Electronic Requirements for Macropolyhedral Boranes. *Chem. Rev.* **2002**, *102*, 93–144. [[CrossRef](#)]
39. Mingos, D.M.P. *50th Anniversary of Electron Counting Paradigms for Polyhedral Molecules—Historical and Recent Developments (Structure and Bonding)*; Springer Nature: Berlin, Germany, 2021; Volume 187.
40. Mingos, D.M.P. *50th Anniversary of Electron Counting Paradigms for Polyhedral Molecules—Historical and Recent Developments (Structure and Bonding)*; Springer Nature: Berlin, Germany, 2021; Volume 188.
41. Kennedy, J.D. The Polyhedral Metallaboranes. *Prog. Inorg. Chem.* **1984**, *32*, 519–679.
42. Bould, J.; Pasiaka, M.; Braddock-Wilking, J.; Rath, N.P.; Barton, L. Synthesis of Heterobimetallaboranes and Related Species from [(PPh₃)₂(CO)OsB₅H₉]: Pileo-[(PPh₃)₂(CO)OsB₅H₅IrH(PPh₃)(CO)], *closo*-[(PPh₃)₂(CO)(μ-H)OsB₄H₅{η⁵-(C₅Me₅)M}] (M = Rh, Ir), *nido*-[(PPh₃)₂(CO)Os(μ-H){η⁵-(C₅Me₅)Ir}B₃H₆], and *nido*-[(PPh₃)₂(CO)OsB₄H₇(*n*-C₄H₉)]. *Organometallics* **1995**, *14*, 5138–5149.
43. Barton, L.; Bould, J.; Fang, H.; Rath, N.P. Formation of Heterobimetallaheptaboranes from the *nido*-metallahexaboranes (PPh₃)₂(CO)OsB₅H₉ and (PPh₃)₂(CO)IrB₅H₈. *Main Group Met. Chem.* **1996**, *19*, 711–726. [[CrossRef](#)]
44. Bullick, H.J.; Grebenik, P.D.; Green, M.L.H.; Hughes, A.K.; Leach, J.B.; Mountford, P. Reactivity of *nido*-[2-[Fe(η-C₅H₅)]B₅H₁₀] with some transition-metal hydride complexes. *J. Chem. Soc. Dalton Trans.* **1994**, 3337–3342. [[CrossRef](#)]
45. Hoffmann, R. Building Bridges Between Inorganic and Organic Chemistry (Nobel Lecture). *Angew. Chem. Int. Ed. Engl.* **1982**, *21*, 711–724. [[CrossRef](#)]
46. Geetharani, K.; Bose, S.K.; Varghese, B.; Ghosh, S. From Metallaborane to Borylene Complexes: Syntheses and Structures of Triply Bridged Ruthenium and Tantalum Borylene Complexes. *Chem. Eur. J.* **2010**, *16*, 11357–11366. [[CrossRef](#)] [[PubMed](#)]
47. Yuvaraj, K.; Bhattacharyya, M.; Prakash, R.; Ramkumar, V.; Ghosh, S. New Trinuclear Complexes of Group 6, 8, and 9 Metals with a Triply Bridging Borylene Ligand. *Chem. Eur. J.* **2016**, *22*, 8889–8896. [[CrossRef](#)] [[PubMed](#)]
48. Lei, X.; Shang, M.; Fehlner, T.P. Chemistry of Dimetallaboranes Derived from the Reaction of [Cp**M*Cl₂]₂ with Monoboranes (M = Ru, Rh; Cp* = η⁵-C₅Me₅). *J. Am. Chem. Soc.* **1999**, *121*, 1275–1287. [[CrossRef](#)]
49. Pradhan, A.N.; Jaiswal, S.; Ghosh, S. Metal-Rich Metallaboranes: Synthesis, Structure, and Bonding of Heteronuclear Trimetallic Clusters containing (μ₃-BH) Ligand. *Eur. J. Inorg. Chem.* **2023**, *26*, e202300254–e202300263. [[CrossRef](#)]
50. Pradhan, A.N.; Bairagi, S.; Ghosh, S. Diborane and Triborane Species in the Coordination Sphere of Group-8 Transition Metals. *Inorg. Chem.* **2023**, *62*, 14790–14803. [[CrossRef](#)]
51. Lei, X.; Shang, M.; Fehlner, T.P. Synthesis and Characterization of Cp*₃Ru₃B₃H₈, Cp* = η⁵-C₅Me₅, Exhibiting a Capped *Nido* Geometry. Cluster Geometry Driven by Hydrogen Bridging. *Inorg. Chem.* **1998**, *37*, 3900–3901. [[CrossRef](#)]
52. Bhattacharyya, M.; Prakash, R.; Jagan, R.; Ghosh, S. Synthesis and ligand substitution of tri-metallic triply bridging borylene complexes. *J. Organomet. Chem.* **2018**, *866*, 79–86. [[CrossRef](#)]
53. Chipperfield, A.K.; Housecroft, C.E.; Matthews, D.M. Ru₃(CO)₉B₂H₆: A metal-rich ruthenaborane analogue of pentaborane(9) and a model for a triruthenium supported unsaturated hydrocarbon. *J. Organomet. Chem.* **1990**, *384*, C38–C42. [[CrossRef](#)]
54. Leadbeater, N.E. A High Yield Route to Ruthenaboranes. *Organometallics* **1998**, *17*, 5913–5915. [[CrossRef](#)]
55. Grebenik, P.D.; Green, M.L.H.; Kelland, M.A.; Leach, J.B.; Mountford, P. Synthesis of Small *nido*-Ferrapentaboranes; a Novel Borane-capped *nido*-Diferrapentaborane. Synthesis of Small *nido*-Ferrapentaboranes; a Novel Borane-capped *nido*-Diferrapentaborane. *J. Chem. Soc. Chem. Commun.* **1990**, 1234–1236. [[CrossRef](#)]
56. Hattersley, A.D.; Housecroft, C.E.; Rheingold, A.L. Cluster core geometrical variation in heterometallic boride clusters containing RhRu₄ skeletons: Crystal structures of [RhRu₄H₂(η⁵-C₅Me₅)(μ-Cl)(CO)₁₂B] and [RhRu₄H(nbd)(CO)₁₂B(AuPPh₃)] (nbd = norbornadiene). *J. Chem. Soc. Dalton Trans.* **1996**, *1996*, 603–610. [[CrossRef](#)]
57. Ghosh, S.; Fehlner, T.P.; Beatty, A.M.; Noll, B.C. Insertion of B-X (X = Cl, SMe₂) Moieties into Ruthenaborane Frameworks: Synthesis and Characterization of (η⁵-C₅Me₅Ru)₂(μ-H)B₄H_mCl_n, (m, n = 4, 3; 5, 2; 7, 2), *closo*-1-(SMe₂)-2,3-(η⁵-C₅Me₅Ru)₂(μ₃-H)B₅HCl₃, and *closo*-2,3-(η⁵-C₅Me₅Ru)₂B₆H₃Cl₃. *Organometallics* **2005**, *24*, 2473–2480. [[CrossRef](#)]

58. Mondal, B.; Bag, R.; Ghorai, S.; Bakthavachalam, K.; Jemmis, E.D.; Ghosh, S. Synthesis, Structure, Bonding, and Reactivity of Metal Complexes Comprising Diborane(4) and Diborene(2): $[\{\text{Cp}^*\text{M}(\text{CO})_2\}_2\{\mu\text{-}\eta^2\text{:}\eta^2\text{-B}_2\text{H}_4\}]$ and $[\{\text{Cp}^*\text{M}(\text{CO})_2\}_2\text{B}_2\text{H}_2\text{M}(\text{CO})_4]$, M = Mo, W. *Angew. Chem. Int. Ed.* **2018**, *57*, 8079–8083. [[CrossRef](#)] [[PubMed](#)]
59. Sharmila, D.; Mondal, B.; Ramalakshmi, R.; Kundu, S.; Varghese, B.; Ghosh, S. First-row Transition Metal-Diborane and Borylene Complexes. *Chem. Eur. J.* **2015**, *21*, 5074–5083. [[CrossRef](#)] [[PubMed](#)]
60. Anju, R.S.; Saha, K.; Mondal, B.; Dorcet, V.; Roisnel, T.; Halet, J.F.; Ghosh, S. Chemistry of Diruthenium Analogue of Pentaborane(9) With Heterocumulenes: Toward Novel Trimetallic Cubane-Type Clusters. *Inorg. Chem.* **2014**, *53*, 10527–10535. [[CrossRef](#)]
61. Ryschkewitsch, G.E.; Nainan, K.C. Octahydrotriborate(1-) ($[\text{B}_3\text{H}_8]^-$) salts. Method A. *Inorg. Synth.* **1974**, *15*, 113–114.
62. Weiss, R.; Grimes, R.N. Sources of Line Width in Boron-11 Nuclear Magnetic Resonance Spectra. Scalar Relaxation and Boron-Boron Coupling in B_4H_{10} and B_5H_9 . *J. Am. Chem. Soc.* **1978**, *100*, 1401–1405. [[CrossRef](#)]
63. Led, J.J.; Gesmar, H. Application of the linear prediction method to NMR spectroscopy. *Chem. Rev.* **1991**, *91*, 1413–1426. [[CrossRef](#)]
64. Altomare, A.; Cascarano, G.; Giacovazzo, C.; Guagliardi, A.; Burla, M.C.; Polidori, G.; Camalli, M. SIRPOW. 92—A program for automatic solution of crystal structures by direct methods optimized for powder data. *J. Appl. Cryst.* **1994**, *27*, 435–436. [[CrossRef](#)]
65. Sheldrick, G.M. SHELXT—Crystal structure refinement with SHELXL. *Acta Cryst.* **2015**, *71*, 3–8.
66. Sheldrick, G.M. *SHELXS97 and SHELXL97: Program for Crystal Structure Solution and Refinement*; University of Gottingen: Gottingen, Germany, 1997.
67. Dolomanov, O.V.; Bourhis, L.J.; Gildea, R.J.; Howard, J.A.K.; Puschmann, H. OLEX2: A complete structure solution, refinement and analysis program. *J. Appl. Cryst.* **2009**, *42*, 339–341. [[CrossRef](#)]
68. Frisch, M.J.; Trucks, G.W.; Schlegel, H.B.; Scuseria, G.E.; Robb, M.A.; Cheeseman, J.R.; Scalmani, G.; Barone, V.; Petersson, G.A.; Nakatsuji, H.; et al. *Gaussian 16, Revision C.01*; Gaussian, Inc.: Wallingford, CT, USA, 2016.
69. Schmider, H.L.; Becke, A.D. Optimized density functionals from the extended G2 test set. *J. Chem. Phys.* **1998**, *108*, 9624–9631. [[CrossRef](#)]
70. Perdew, J.P. Density-functional approximation for the correlation energy of the inhomogeneous electron gas. *Phys. Rev. B Condens. Matter Mater. Phys.* **1986**, *33*, 8822–8824. [[CrossRef](#)] [[PubMed](#)]
71. Pritchard, B.P.; Altarawy, D.; Didier, B.; Gibson, T.D.; Windus, T.L. A New Basis Set Exchange: An Open, up-to-date Resource for the Molecular Sciences Community. *J. Chem. Inf. Model.* **2019**, *59*, 4814–4820. [[CrossRef](#)] [[PubMed](#)]
72. London, F.J. Quantum theory of interatomic currents in aromatic combinations. *J. Phys. Radium* **1937**, *8*, 397–409. [[CrossRef](#)]
73. Wiberg, K. Application of the Pople-Santry-Segal CNDO Method to the Cyclopropylcarbiny1 and Cyclobutyl Cation and to Bicyclobutane. *Tetrahedron* **1968**, *24*, 1083–1096. [[CrossRef](#)]
74. Glendening, E.D.; Badenhoop, J.K.; Reed, A.E.; Carpenter, J.E.; Bohmann, J.A.; Morales, C.M.; Landis, C.R.; Weinhold, F. *NBO Program 6.0*; Theoretical Chemistry Institute, University of Wisconsin: Madison, WI, USA, 2013.
75. Lu, T.; Chen, F. Multiwfn: A multifunctional wavefunction analyzer. *J. Comput. Chem.* **2012**, *33*, 580–592. [[CrossRef](#)]

Disclaimer/Publisher’s Note: The statements, opinions and data contained in all publications are solely those of the individual author(s) and contributor(s) and not of MDPI and/or the editor(s). MDPI and/or the editor(s) disclaim responsibility for any injury to people or property resulting from any ideas, methods, instructions or products referred to in the content.